





# Synthesis of Graphene Quantum Dot Zinc Oxide Nanocomposites: Assessment of their Antioxidant and Antimicrobial Activity

Oskay Kahraman <sup>1</sup>, Ersan Turunc <sup>2\*</sup>, Aylin Dogen <sup>3</sup>, Rıza Binzet <sup>4</sup>

<sup>1</sup> Department of Biology, Faculty of Science, Mersin University, 33343, Mersin, Turkey; oskaykahraman@gmail.com (O.K.);

<sup>2</sup> Department of Chemistry and Chemical Processing Technologies, Technical Science Vocational School, Mersin University, Mersin 33343, Turkey; ersanturunc@mersin.edu.tr (E.T.);

<sup>3</sup> Department of Pharmaceutical Microbiology, Faculty of Pharmacy, Mersin University, 33160, Mersin, Turkey; aylinats@mersin.edu.tr (A.D.);

<sup>4</sup> Department of Biology, Faculty of Science, Mersin University, 33343, Mersin, Turkey; rbinzet@mersin.edu.tr (R.B.);

\* Correspondence: ersanturunc@mersin.edu.tr (E.T.);

Scopus Author ID 6503917811

Received: 11.01.2023; Accepted: 23.02.2023; Published: 2.02.2024

**Abstract:** Graphene quantum dots zinc oxide (GQDs/ZnO) nanocomposites were prepared using simple, non-toxic, economical synthesis routes. The synthesized structures were characterized by UV-Vis spectroscopy, X-ray diffraction (XRD), Scanning electron microscope (SEM), Transmission electron microscopy (TEM), X-ray photoelectron spectroscopy (XPS), and Malvern Zeta Sizer. To determine the reducing potential of the nanostructures obtained in this study, the reducing power activity test, DPPH, and hydrogen peroxide scavenging activity tests were carried out to determine their antioxidant properties. Moreover, the xanthine oxidase inhibitory activity of GQDs/ZnO was investigated. The results showed that GQDs/ZnO nanocomposites have strong xanthine oxidase inhibitor activity. In this study, the antimicrobial activity of GQDs/ZnO nanocomposite was also investigated against Gram(+), Gram(-), and fungal strains. GQDs/ZnO nanocomposites showed different antimicrobial activity depending on these bacterial and fungal strains.

**Keywords:** graphene quantum dot; zinc oxide; nanocomposite; antioxidant; antimicrobial.

© 2024 by the authors. This article is an open-access article distributed under the terms and conditions of the Creative Commons Attribution (CC BY) license (<https://creativecommons.org/licenses/by/4.0/>).

## 1. Introduction

Graphene has attracted the scientific world's attention recently due to its excellent thermal, electronic, physical, and mechanical properties [1-4]. Graphene quantum dots (GQDs), which are in the class of graphene materials, are an alternative to graphene with some of their properties. GQDs have outstanding characteristics due to the large surface area, p-p conjugated network system, and due to the contents of various surface groups [5]. Also, GQDs have photoluminescence compared to graphene. Furthermore, GQDs have stable fluorescence, good solubility in water, excellent biocompatibility, and low toxicity [6-10]. GQDs have potential uses in different areas due to their properties, such as biosensing [11], bioimaging [12], photocatalysis [13], energy storage [14], and drug delivery [15]. GQDs have been synthesized via various techniques, such as microwave-assisted hydrothermal [16], electrochemical [17], and electron beam lithography [18]. Also, it has been synthesized using various carbon sources like glucose, graphite, coal, and toner residue [19-22]. These methods

generally have some disadvantages, such as low reaction efficiency, use of toxic chemicals, and high cost [23,24]. In order to eliminate these disadvantages, researchers have tried to develop different synthesis methods. Plants are natural carbon sources due to they contain phytochemicals. The use of plants in synthesizing GQDs offers advantages such as being cheap compared to other methods, high reaction efficiency, and not using toxic chemicals. Zinc oxide nanostructure is a semiconductor material with excellent properties such as high redox potential, large surface area, non-toxicity, low cost, and large band gap (3.37 eV) [25,26]. The literature review shows that graphene quantum dot zinc oxide nanocomposites have been synthesized using different methods [27-31].

A free radical is a highly active substance due to the contain unpaired one or more unpaired electrons [32,33]. Reactive oxygen species (ROS) play various roles in biological systems. Free radicals may produce by various sources [34]. They participate in cellular signaling pathways when they are present in appropriate amounts in cells. However, in excess, they have negative effects on biological systems [35]. The excess of the reactive oxygen species plays a role in the development or pathophysiology of diseases such as cancer, diabetes, and Parkinson's and causes aging [36]. Therefore, keeping or destroying reactive oxygen species at the appropriate level in the cells is very important. Antioxidant molecules can reduce them to an appropriate level or destroy the cells' free radicals and prevent them against excess free radicals [37].

Bacterial infectious diseases are increasing all over the world and pose a serious threat to human health [38]. Also, bacteria can be resistant to antibiotics with the times. The evolution rate of bacterial drug resistance is expected to hold down the research and decrease the development of new antibiotics with the increase in cost [39]. Therefore there most important is finding new and effective antimicrobials. In recent years, metal oxide nanoparticles have been used as effective and potent antimicrobial agents [40-43]. Nanoparticles can easily penetrate the bacterial surface and form reactive oxygen species by damaging membrane and cell components such as DNA, lipids, and proteins [44].

*Sarcopoterium spinosum* (L.) Spach used in this study belongs to the Rosaceae family. *S. spinosum* is distributed in the eastern Mediterranean region [45]. Its branches are wooden, end in branched thorns, and grow to a length of 30-40 cm [46]. Various part of the *S. spinosum* has been known to utilize treatment of various diseases like cancer, diabetes, digestive problem, and pain relief [47,48].

In this study, we aimed to reveal the antimicrobial and antioxidant potential of GQDs/ZnO nanocomposite structures. For this purpose, we synthesized GQDs using *S. spinosum* fruit powder as a carbon source. Then we synthesized GQDs/ZnO by using a simple and economical synthesis route.

## 2. Materials and Methods

### 2.1. Chemicals.

All chemicals are analytical grade.  $Zn(CH_3COO)_2 \cdot 2H_2O$ , xanthine, and Xanthine oxidase enzyme solution from Bovine milk serum were purchased from Sigma Aldrich. Hydrogen peroxide, 2,2-Diphenyl-1-picrylhydrazyl (DPPH), potassium hexacyanoferrate, sodium chloride, and potassium dihydrogen phosphate were purchased from Merck.

## 2.2. Characterization techniques and instrumentations.

The formation of the GQDs/ZnO nanocomposite structure was investigated by using a UV-Vis spectrophotometer (Shimadzu 1800 spectrophotometer), and the crystal structure was determined by X-ray powder diffraction (XRD). The surface morphology, shape, and elemental compositions were performed by Transmission Electron Microscope (JEOL JEM 1011 Megaview III Camera iTEM Software), Scanning Electron Microscope (FEI Quanta 650 FEG SEM), Energy dispersive X-Ray diffraction meter (EDS). The particle size and surface charge of nanocomposites were determined via Malvern zeta sizer, and the chemical state was investigated by X-ray photoelectron spectroscopy (XPS).

## 2.3. Preparation of plant extract.

*S. spinosum* fresh fruits were collected from Mersin University, Ciftlikkoy Campus (Collection stations: Mersin University, Ciftlikkoy Campus, maquis degraded areas, 100-130 m). The collected fruits of *S. spinosum* were air-dried in the shade at room temperature (25 °C) for a month. Then, the dried fruits were powdered using a grinder (Blender 8011ES Model HGB2WTS3 400 W). Fruit powder was stored in a sterile dark bottle at room temperature until extraction studies.

## 2.4. Synthesis of GQDs/ZnO nanocomposites.

One (1.0) gram of fruit powder of *S. spinosum* was placed in a crucible and taken in a muffle furnace. The fruit powder was calcinated at 350 °C for 2 hours. Next, the resulting powder was mixed with 100 mL of distilled water and boiled at about 90 °C for 2 hours. After 2 hours, the mixture was cooled to room temperature. Then the mixture was centrifuged at 6000 rpm for 15 minutes. The supernatant was filtered using a 0.22 µm syringe filter. Finally, the filtered part was lyophilized and stored at room conditions for further studies.

For the synthesis of GQDs/ZnO nanocomposites, 10 mL of GQDs were taken in a bottle. To this solution, 0.0219 g  $\text{Zn}(\text{CH}_3\text{COO})_2 \cdot 2\text{H}_2\text{O}$  (10.0 mM) was added with stirring. The pH of the solution was then adjusted to 11 with 2.0 M NaOH. This mixture was stirred at 80-85 °C for 5 hours. After 5 hours, the reaction mixture was cooled to room temperature and centrifuged at 6000 rpm for 15 minutes thrice. The obtained solid product was dried at 60 °C in the oven.

## 2.5. Antioxidant Activity of GQDs/ZnO nanocomposites.

### 2.5.1. DPPH radical scavenging activity assay.

We determined the antioxidant activity of GQDs/ZnO nanocomposites using the method used by Zhao *et al.* [17]. GQDs/ZnO nanocomposites (62.5 - 1000 µg/mL) were mixed with 1 mL of freshly prepared DPPH methanolic solution (0.05 mg/mL) and incubated for 1 hour at room temperature in the dark. After the incubation period, the absorption of the solution was measured at 515 nm. The antioxidant activity of the GQDs/ZnO nanocomposite structure was evaluated using the formula at  $1 - (\text{Cc}/\text{Cs}) * 100$ . Cc and Cs refer to the DPPH radical without and with samples. Ascorbic acid was used as a positive control, and methanol was used as a blank group. All tests were performed three times.

### 2.5.2. Hydrogen peroxide scavenging assay.

The ability of the GQDs/ZnO nanocomposites to scavenge hydrogen peroxide (H<sub>2</sub>O<sub>2</sub>) was determined by a modification to the method of Ruch *et al.* [49]. 1 mL of GQDs/ZnO nanocomposite (40 - 100 µg/mL) was transferred to vials, and their volume was brought to 2 mL with PBS (pH = 7.4), followed by the addition of H<sub>2</sub>O<sub>2</sub> (40 mM, 0.6 mL) solution prepared with PBS. The reaction mixture was stirred for a few seconds, and after 10 min of incubation time, its absorbance was measured at 230 nm. Ascorbic acid and phosphate buffers were used as the positive control and blank. The ability of the extracts to scavenge the H<sub>2</sub>O<sub>2</sub> was calculated using the following equation:

$$\% \text{ Scavenging assay} = [(Ac-As)/Ac]*100 \quad (1)$$

Ac refers to the H<sub>2</sub>O<sub>2</sub> solution in the phosphate buffer (pH 7.4), and As refers to H<sub>2</sub>O<sub>2</sub>-added sample solutions. All tests were performed three times.

### 2.5.3. Reducing power assay.

The reducing power potential of the GQDs/ZnO nanocomposite was determined based on the method determined by Hue [50]. Different concentrations of samples (62.5-1000 µg/mL) were prepared and separately mixed with 2.5 mL phosphate buffer (0.2 M, pH 6.6) and 2.5 mL of potassium ferricyanide (1 %). The mixtures were incubated at 50 °C for 20 min in a water bath. Then 2.5 mL of trichloroacetic acid (TCA) (10 %) was added to the mixtures, which were then centrifuged at 3.000 rpm for 10 min. After, the 2.5 mL supernatant solutions (upper layer) were taken to the bottles and mixed with 0.5 mL FeCl<sub>3</sub> (0.1 %). After 10 minutes, absorbances were measured at 700 nm in a UV-Vis spectrophotometer. All tests were repeated three times. All solutions were freshly prepared.

### 2.5.4. Xanthine oxidase inhibition assay.

Xanthine oxidase activity of GQDs/ZnO nanocomposites was determined by measuring uric acid formation from xanthine using the method Saghal [51]. Briefly, GQDs/ZnO nanocomposites were dissolved in 50 mM phosphate buffer (pH = 7). Various concentrations of GQDs/ZnO (62.5-1000 µg/mL) were added to 1 mL xanthine solutions (150 mM). Then these reaction mixtures were incubated at room temperature for 15 minutes. After 15 minutes, the xanthine oxidase enzyme solution (0.4 U/mL) was added to mixtures and incubated for 15 minutes. After the incubation, uric acid production was determined by measuring the absorbances at 295 nm. Xanthine oxidase activity was expressed as the percentage inhibition of xanthine oxidase, calculated by Eq. 1. The samples without GQDs/ZnO nanocomposite were used as Allopurinol was used as a positive control. Xanthine and xanthine oxidase enzyme solutions were prepared as phosphate buffers. One unit of xanthine oxidase was determined as the amount of enzyme required to produce 1 mmol of uric acid/minute at room temperature.

### 2.6. Antimicrobial activity of GQDs/ ZnO nanocomposite.

In vitro, the antimicrobial activities of the synthesized GQDs/ZnO nanocomposites were tested against Gram-positive and Gram-negative bacteria and fungi. The antimicrobial susceptibility test was evaluated using the modification microdilution broth method [52]. Antibacterial activities of the synthesized GQDs/ZnO nanocomposites have been tested against different types of bacteria and fungi. In the present study, the tested Gram(+) are *Staphylococcus aureus* (ATCC 29213), *Streptococcus pneumoniae* (ATCC 49619), <https://biointerfaceresearch.com/>

*Enterococcus faecalis* (ATCC 29212), and the Gram(-) bacteria are *Escherichia coli* (ATCC 25922), *Klebsiella pneumoniae* (ATCC BAA-1901), *Pseudomonas aeruginosa* (ATCC 27853). Besides, the tested fungi are *Candida metapsilosis* (CBS 2916) and *Candida parapsilosis* (ATCC 22019). The fungal and bacterial cell inoculum was prepared from the stock culture grown in Tryptic Soy Agar (TSA, Merck, Darmstadt, Germany) at 28 °C for 24 h and Mueller-Hinton Agar (MHA, Merck, Darmstadt, Germany) 37 °C for 24 h, respectively. The cell density adjusts to match the turbidity of a Mac Farland 0.5. Antibacterial and antifungal activity tests were performed in Mueller-Hinton broth (Merck, Darmstadt, Germany) and Tryptic soy broth (Merck, Darmstadt, Germany), respectively. Dilutions of GQDs/ZnO nanocomposites and standard drugs in the test medium were prepared in serial dilutions; 500, 250, 125,... µg/mL concentration with Mueller-Hinton broth and Tryptic soy broth. Then 5 µL of cell suspension was added to each tube, except the last one, which acted as a control well. Only 5 µL of fungal and bacterial suspension were added in another control tube without chemicals and used as a control for growing. All plates were incubated at 28 °C (for fungi) and 37 °C (for bacteria) for 24 h. Minimum inhibitory concentration (MIC) values were recorded on the lowest concentrations of the compounds, which had no visible turbidity for bacteria and fungi. Ampicillin and fluconazole were used as reference drugs in antibacterial and antifungal activity tests, respectively. The results were obtained visually and by measuring optical density for 24 hours.

### 3. Results and Discussion

In this study, we have synthesized GQDs/ZnO nanocomposites using a simple, non-toxic, and economical synthesis route. *S. spinosum* fruit powder is used as raw material for GQD synthesis (Figures 1a and b).

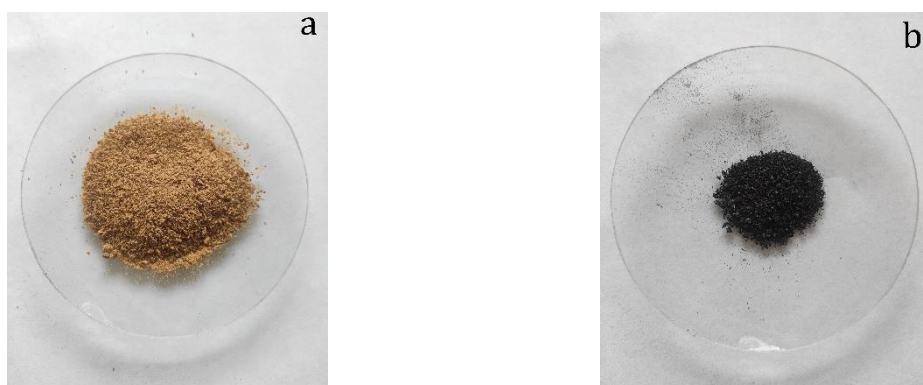


**Figure 1.** (a) *S. spinosum* fruit powder; (b) the carbonized form of *S. spinosum* fruit powder.

Reaction yield (carbonization percent) is calculated by using the following equation:

$$\text{Reaction yield} = [(\text{Initial amount} - \text{final amount}) / \text{initial amount}] * 100 \quad (2)$$

In our work, the reaction yield (carbonization percent) is calculated as 22.2 %.

#### 3.1. Optical characteristics.

The absorption peak seen at 228 nm and the weak peak seen at 302 nm in the UV-Vis spectrum correspond to the  $\pi$ - $\pi^*$  transition of aromatic  $sp^2$  and n-  $\pi^*$  transition of C=O domains. This result indicates the formation of GQDs structure from *S. spinosum* fruit powder. The absorption peak formed at 375 nm indicates the formation of the GQDs/ZnO structure (Figure 2).

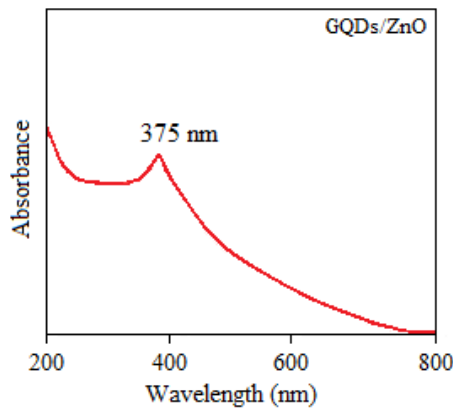


**Figure 2.** The UV-Vis spectra of GQDs/ZnO nanocomposite.

3.2. X-ray diffraction (XRD) of GQDs/ZnO nanocomposite.

XRD pattern for the synthesized GQDs/ZnO nanocomposite display series of diffraction peaks at  $2\theta = 31.79^\circ, 34.47^\circ, 36.27^\circ, 47.54^\circ, 56.64^\circ, 62.82^\circ, 67.93^\circ, 69.06^\circ, 77.1^\circ$  which can be assigned to the (100), (002), (101), (102), (110), (103), (112), (201) and (202) planes of hexagonal wurtzite ZnO nanostructure, respectively (JCPDS card no. 36-1451) [53] (Figure 3).

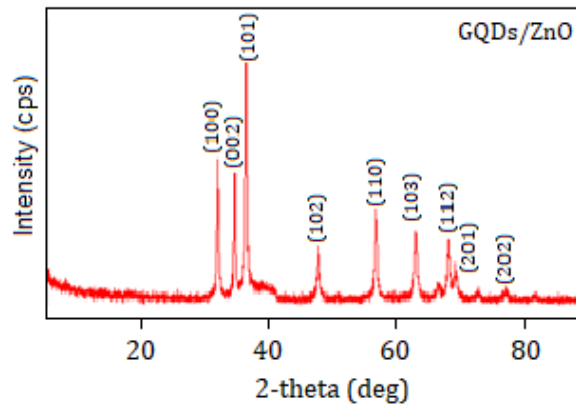


**Figure 3.** XRD of GQDs/ZnO nanocomposite.

The crystallite size of GQDs/ZnO nanocomposite was calculated from XRD results by the Debye-Scherrer equations (Eq. 3), and the average crystallite size of synthesized GQDs/ZnO nanocomposite structures was determined as 34.4 nm.

$$\text{Crystallite size} = k\lambda/\beta \cos \theta \tag{3}$$

$k$  is the theoretical value at 0.9.  $\lambda$  is the X-ray diffraction wavelength ( $0.154 \text{ \AA}$ ).  $\beta$  is the corresponding value of the full width at half maximum (FWHM), and  $\theta$  is the plane's position.

Bragg equations (Eq. 4) were used to calculate the interlayer distance ( $d$  spacing) value for the GQDs/ZnO nanocomposite.

$$n\lambda = 2d\sin\theta \tag{4}$$

The theoretical  $d$ -spacing value of the graphitic carbon is approximately 0.34 nm [54]. The calculated  $d$  spacing of the GQDs/ZnO nanocomposites structures is 0.24 nm. Interlayer distance ( $d$  spacing) decreased in the case of GQDs/ZnO nanocomposite structure. This result confirms the successful incorporation of GQDs and ZnO nanostructure in the GQDs/ZnO nanocomposite.

The lattice parameters, including the lattice constant ( $a$  and  $c$ ), were calculated based on the XRD results. The lattice constants  $a$  and  $c$  were calculated using Eq. 5 and 6,

corresponding to the (100) and (002) planes. The calculated lattice parameter shows in Table 1.

$$a = \lambda/\sqrt{3} \times \sin\Theta \tag{5}$$

$$c = \lambda/\sin\Theta \tag{6}$$

**Table 1.** Calculated lattice constant for GQDs/ZnO nanocomposites.

Samples	c value (Å°)	a value (Å°)	c/a value (Å°)
GQDs/ZnO	5.31	3.25	1.63
JCPDS	5.21	3.25	1.60

The c/a ratio of the GQDs/ZnO nanocomposite structure is 1.63 Å°, which is greater than the standard value. This may be due to the fast crystallization of ZnO nanostructures on the surface of GQDs.

### 3.3. Structural characterization.

The surface morphology, structural property, and chemical content of the obtained GQDs/ZnO nanocomposites were determined via SEM, TEM, and EDX. The SEM image clearly shows that ZnO nanoparticles were homogeneously dispersed on the surface of the GQDs during synthesis (Figure 4a).

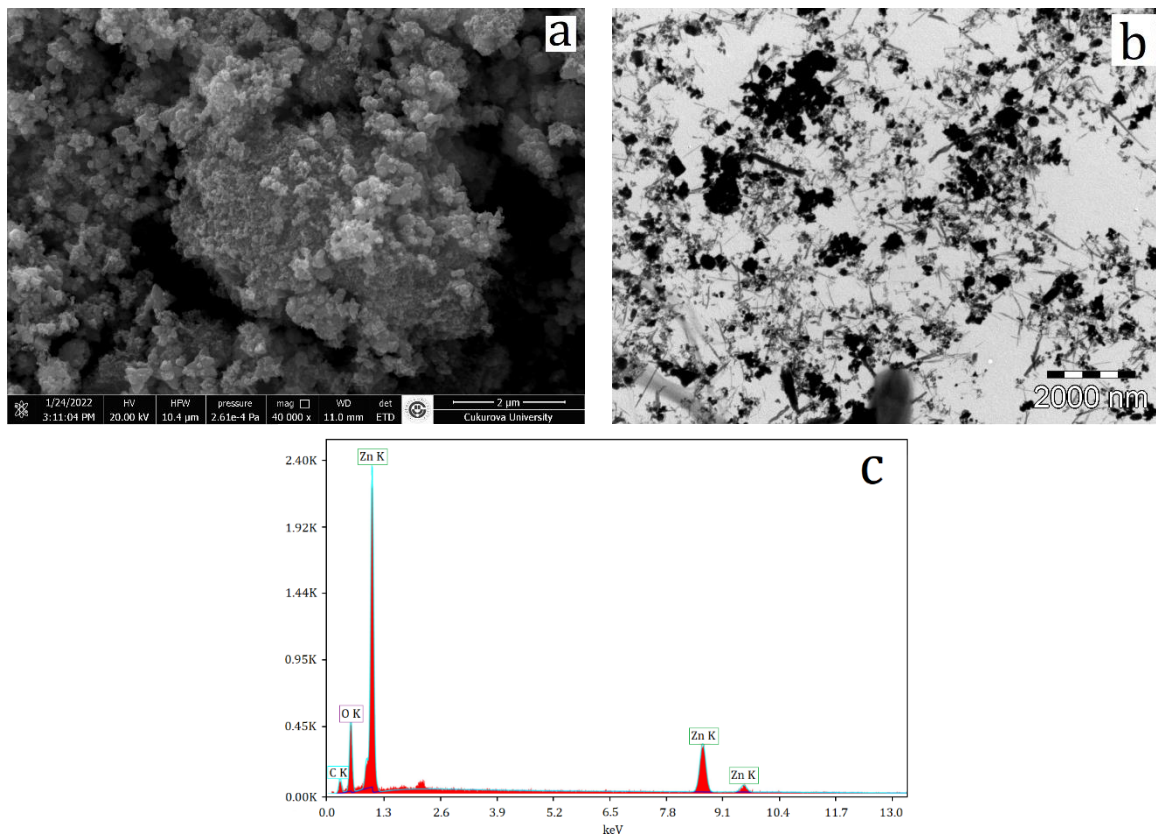


**Figure 4.** (a) SEM and (b) TEM images, and (c) EDX spectra of GQD/ZnO nanocomposites.

TEM micrograph showed that with the formation of GQDs/ZnO nanocomposites, a large number of ZnO nanoparticles adhered and aggregated on the surface of GQDs (Figure 4b). The elemental composition of the GQDs/ZnO nanocomposite was determined by EDX. Carbon (C), oxygen (O), and zinc (Zn) were detected on the surface of the GQDs/ZnO nanocomposite. Therefore, the presence of C, O, and Zn indicates the formation of the GQDs/ZnO nanocomposite structure. The elemental composition of the GQDs/ZnO

nanocomposite structure is 15.2%, 26.39%, and 58.42% for C, O, and Zn, respectively (Figure 4c).

### 3.4. Particle size and zeta potential of GQDs/ZnO nanocomposites.

Particle size and zeta potential of GQDs/ZnO nanocomposites were determined by the DLS technique. The value of zeta potential gives knowledge about the short or long-term stability of GQDs/ZnO particles in an aqueous medium. GQDs/ZnO surface charge was determined as -14.6 mV (Figure 5a). DLS analysis suggests that the GQDs/ZnO nanocomposite aqueous solution has stability for a long time period. The particle size of GQDs/ZnO nanocomposite was measured at 56.24 nm (Figure 5b). The increase in particle size may be due to the aggregation of ZnO structures formed during the synthesis on the GQDs surface.

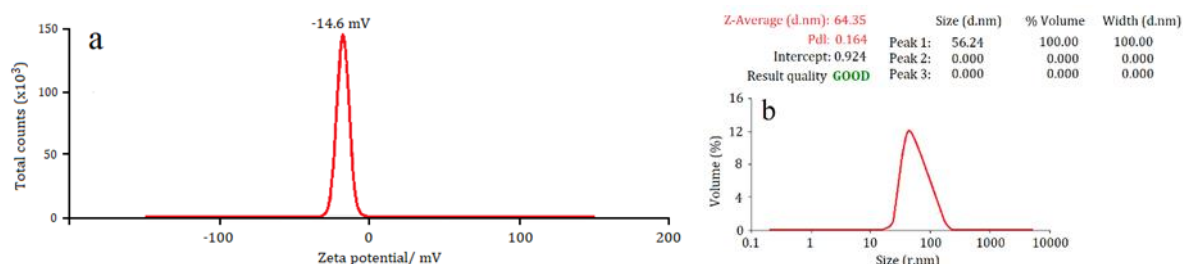


**Figure 5.** Zeta potential (a) and particle size (b) of GQDs/ZnO.

### 3.5. X-ray photoelectron spectroscopy (XPS) analysis.

XPS analysis was performed to determine the elemental composition and chemical state of the GQDs/ZnO composites. The XPS survey spectrum of GQDs/ZnO is given in Figure 6a. Three characteristic peaks correspond to C 1s, O 1s, and Zn 2p, respectively. Figure 6b shows the high-resolution C 1s spectrum can be deconvoluted into two peaks at binding energies of 285.58 eV and 289.69 for sp<sup>2</sup>-C and C=O, respectively [55]. The O 1s spectrum (Figure 6c) consists of one peak at the binding energy of 531.38 eV corresponds to C=O (carbonyl and carboxyl) [56-58]. The high-resolution XPS spectra of Zn 2p demonstrate two main peaks at 1022.48 eV and 1045.58 eV correspond to Zn 2p<sub>3/2</sub> and 2p<sub>1/2</sub> (Figure 6d), respectively [59]. These results demonstrate the successful incorporation of Zn into GQDs.

### 3.6. Antioxidant activity.

#### 3.6.1. DPPH scavenging assay.

Antioxidant activities were measured by a 2,2-diphenyl-2-picrylhydrazyl (DPPH) radical-scavenging assay according to the method described by Zhao [17]. In this study, we investigated the antioxidant activity of the GQDs/ZnO nanocomposite. Our results show that the synthesized GQDs/ZnO nanocomposites have moderate antioxidant activity (Figure 7). As seen in Figure 7, DPPH radical scavenging activities were 31.8 % and 80.6 % for GQDs/ZnO and ascorbic acid at 1000 µg/mL, respectively. It is thought that the GQDs/ZnO nanocomposite does not donate enough electrons or H-atoms to the DPPH molecule due to its chemical structure.



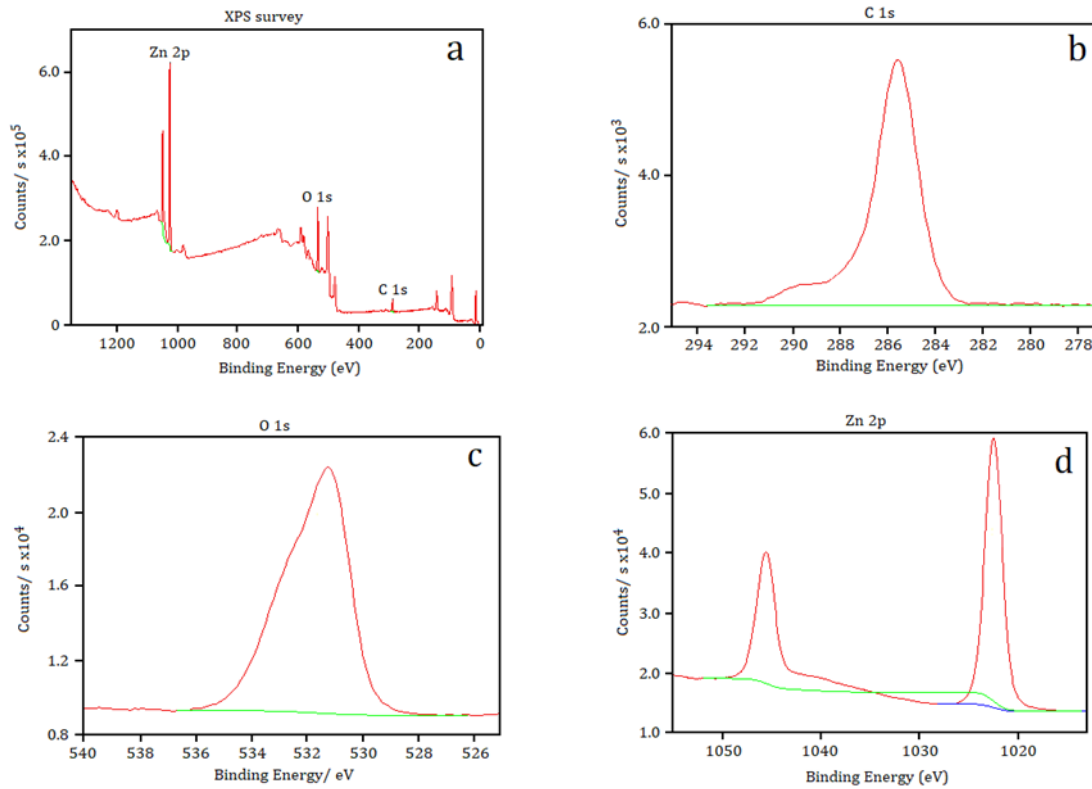


**Figure 6.** (a) XPS survey spectra of GQDs/ZnO composite, and high-resolution XPS spectra of (b) C 1s, (c) O 1s, and (d) Zn 2p.

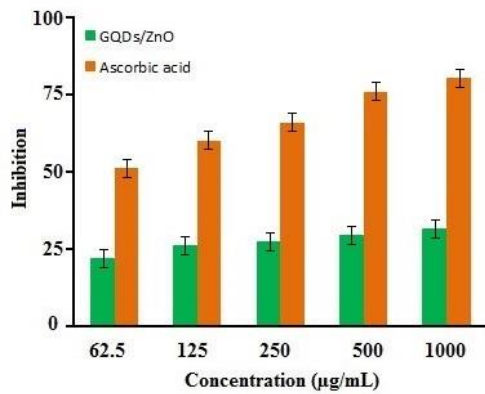


**Figure 7.** The DPPH scavenging activity of samples.

### 3.6.2. Hydrogen peroxide scavenging assay.

H<sub>2</sub>O<sub>2</sub> is not toxic to living organisms in low amounts. However, H<sub>2</sub>O<sub>2</sub> can produce hydroxyl (HO<sup>•</sup>) radicals or superoxide radicals (O<sub>2</sub><sup>•-</sup>) in various reactions such as Fenton or Haber-Weiss reactions [60]. The hydroxyl or superoxide radical creates a toxic effect on cells due to its involvement in various reactions in metabolism. Therefore it is extremely important to eliminate the H<sub>2</sub>O<sub>2</sub> radical accumulated in the cells. In our results, the synthesized GQDs/ZnO nanocomposites have good H<sub>2</sub>O<sub>2</sub> scavenging activity (Fig. 8). The H<sub>2</sub>O<sub>2</sub> scavenging activity was 62.58 % and 68.20 % for GQDs/ZnO and ascorbic acid at 100 µg/mL, respectively. The enzymes using zinc as a cofactor scavenge H<sub>2</sub>O<sub>2</sub> free radicals, and the presence of zinc in the nanocomposite structure may be responsible for the improved H<sub>2</sub>O<sub>2</sub> free radical scavenging activity.

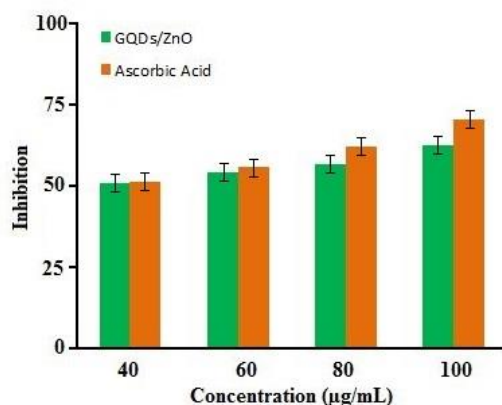


**Figure 8.** Hydrogen peroxide scavenging activity of samples.

### 3.6.3. Reducing power activity.

The ability of antioxidants to donate an electron or H<sup>•</sup> atom can be measured by the reducing power assay. Reducing power assay is based on the reaction of samples with potassium ferricyanide to produce potassium ferrocyanide, followed by a reaction with ferric chloride (FeCl<sub>3</sub>) to form a ferric-ferrous complex has an absorbance maximum at 700 nm [61]. Higher absorbance values indicate higher reducing ability. The absorbance values of the samples at 700 nm are given in Table 2. Ascorbic acid reduces power activity more than GQDs/ZnO nanocomposites (Figure 9).

**Table 2.** The absorbance value of samples.

Concentration (µg/mL)	GQDs/ZnO	Ascorbic acid
62.5	0.174	0.350
125	0.179	0.482
250	0.183	0.653
500	0.191	0.826
1000	0.284	1.210

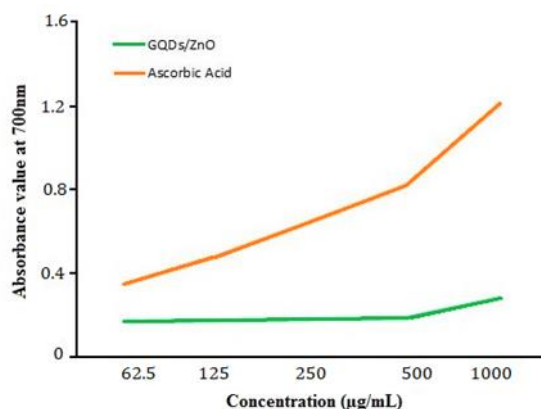
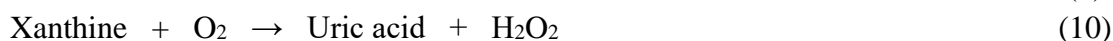
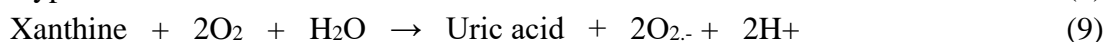


**Figure 9.** The absorbance of GQDs/ZnO and ascorbic acid at 700 nm.

### 3.6.4. Xanthine oxidase inhibition activity.

Xanthine oxidase enzyme contains two substrate binding sites, and it catalyzes the oxidation of hypoxanthine to xanthine [62,63]. Excess xanthine causes the formation of uric acid in the body. In addition, oxygen molecules released during the oxidation of xanthine oxidase act as electron acceptors, and superoxide radicals form reactive oxygen species such as hydrogen peroxide [64,65].



The uric acid formed during these reactions is associated with xanthine oxidase activity, and excessive uric acid formation causes highly formation of reactive oxygen species, resulting in oxidative stress. Excess uric acid causes gout disease, rheumatic disease, and acute inflammatory arthritis [66]. Therefore, it is very important to prevent the formation or release of excessive uric acid in the body. Xanthine oxidase inhibitors inhibit uric acid production and may be useful in treating related diseases. The results showed that GQDs/ZnO nanocomposites showed xanthine oxidase inhibitory activity. The xanthine oxidase inhibitor activity was determined at 65.23 % and 80.62 % for GQDs/ZnO and Allopurinol at a concentration of 1000 µg/mL, respectively (Figure 10).

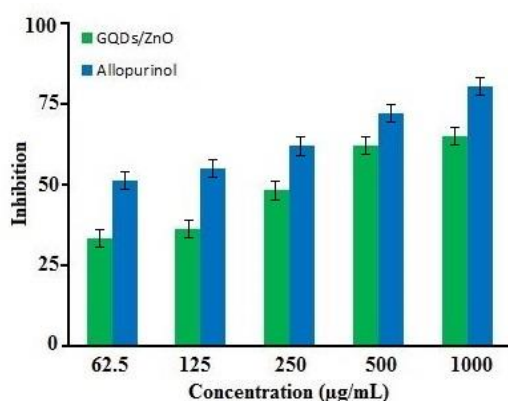


**Figure 10.** Xanthine oxidase inhibition activity of samples.

### 3.7. Antimicrobial activity.

In this study, GQDs/ZnO nanocomposites were tested for antibacterial activities against Gram(+), Gram(-), and fungal strains. The results showed that GQDs/ZnO nanocomposites have antifungal and antibacterial activity. The minimum inhibitor concentration (MIC) values of GQDs/ZnO nanocomposites against bacterial and fungal strains are given in Table 3. GQDs/ZnO nanocomposite can damage bacterial DNA, membrane structure, and cell, and eventually, bacterial death occurs [67]. The antimicrobial activity of nanostructures depends on their size, morphology, and concentration [68]. GQDs/ZnO nanocomposites may show weak or strong antimicrobial activity due to these factors. In this paper, the synergistic effect between the GQDs and ZnONPs has improved antimicrobial activity against *E. coli*, *S. aureus*, and *S. pneumoniae*. After the modification of GQDs with ZnONPs, the rate of separation of electrons and holes produced by ZnONPs under irradiation can increase and produce more reactive oxygen species [69]. GQDs/ZnO nanocomposites have the MIC value of 62.5 µg/mL for *S. aureus*, *S. pneumoniae*, *E. coli*. GQDs/ZnO nanocomposite showed a MIC value of 125 µg/mL against *E. coli*, *P. aureginosa*, and *K. pneumoniae*.

**Table 3** Antimicrobial activity (MIC values) of GQDs/ZnO nanocomposites.

		GQDs/ZnO	Fluconazole	Ampicillin
Gram(+)	<i>S. aureus</i>	62.5	*	-
	<i>S. pneumoniae</i>	62.5	*	-

		GQDs/ZnO	Fluconazole	Ampicillin
Gram(-)	<i>E. faecalis</i>	125	*	-
	<i>E. coli</i>	<b>62.5</b>	*	<b>31.25</b>
	<i>P. aeruginosa</i>	125	*	<b>31.25</b>
	<i>K. pneumoniae</i>	125	*	<b>31.25</b>
Fungi	<i>C. metapsilosis</i>	125	-	*
	<i>C. parapsilosis</i>	125	-	*

-: effective in all concentrations used.

\* : non-effective

Liu *et al.* investigated the antibacterial activity of GQDs/ZnO nanocomposites and polyethyleneimine (PEI) capped GQDs/ZnO nanocomposite structures. The MIC value of the GQDs/ZnO nanocomposite was determined as 4000 µg/mL against *E. coli* [28]. GQDs/ZnO nanocomposites showed the MIC values of 62.5 µg/mL, 125 µg/mL, 62.5µg/mL, 125µg/mL, and 125 µg/mL against *S. aureus*, *E. faecalis*, *E. coli*, *P. aeruginosa*, and *K. pneumoniae*, respectively. Kadian *et al.* reported the synthesis of sulfur-doped GQDs (s-GQDs) and the antimicrobial activity of its against *S. aureus* and *P. aeruginosa*. Depending on the results obtained, MIC values of s-GQDs were reported as > 750 µg/mL against *S. aureus* and *P. aeruginosa* [70]. In this study, the MIC values of GQDs/ZnO against *S. aureus* and *P. aeruginosa* were determined as 125 µg/mL. Rajaura *et al.* synthesized the reduced graphene oxide zinc oxide (rGO-ZnO) nanocomposite and stated that the obtained nanocomposite showed strong antimicrobial activity against *E. coli* [71]. In another study by Usman *et al.*, the antimicrobial activity of rGO-ZnO nanocomposite was investigated against *E. coli* and *S. aureus* and found to be very effective [72]. In a study by Gao *et al.*, the MIC values of the carbon quantum dot/zinc oxide (CQDs/ZnO) composite against *S. aureus* and *E. coli* were determined as 6000 µg/mL and 8000 µg/mL, respectively [73]. In our study, the MIC value of the synthesized GQDs/ZnO nanocomposites was found to be 62.5 µg/mL against *E. coli* and *S. aureus*. It was stated that the CQDs/ZnO nanocomposite obtained in the study by Safardoust did not show inhibitory activity against *S. aureus* and *E. faecalis* [74]. In this paper, the MIC values of the GQDs/ZnO nanocomposite against all tested bacterial strains were determined to be in the range of 62.5 - 250 µg/mL. As a result of all these, we think that the antimicrobial activity of GQDs/ZnO may vary depending on the bacterial species, bacterial membrane structure, interaction with GQDs/ZnO, synthesis route, and chemical components of GQDs/ZnO. It was observed that the GQDs/ZnO nanocomposites obtained in our study show strong antifungal activity against *Candida* species, which is an important factor in candidemias in intensive care units and causes processes that result in high mortality.

#### 4. Conclusions

In this study, GQDs/ZnO nanocomposite were successfully synthesized by a hydrothermal method have synthesized using *S. spinosum* fruit powder. The obtained GQDs/ZnO nanocomposite exhibited antibacterial activity toward all tested organisms. GQDs/ZnO nanocomposite has shown strong antibacterial activity against *S.aureus*, *S. pneumoniae*, and *E. coli*. Due to the synergistic effect between GQDs and ZnO, it may have a more effective antimicrobial effect on these strains. Because ZnO is the main antibacterial component, interfacial charge transfer from GQDs to ZnO facilitates the generation of free radicals. Also, GQDs/ZnO nanocomposite has shown strong antifungal activity against *Candida* species, which is an important factor in candidemia in intensive care units, complicates the intensive care process, and leads to processes that result in high mortality. In

this paper, the synthesized GQDs/ZnO nanocomposite also has antioxidant potential. GQDs/ZnO nanocomposite showed potent xanthine oxidase inhibitory activity. As a result of understanding the toxic effects and antimicrobial and antioxidant mechanisms of nanostructures based on graphene quantum dots, we think that the potential use of these structures will increase, and they will be an alternative to the materials used today.

## Funding

This research received no external funding.

## Acknowledgments

None

## Conflicts of Interest

The authors declare no conflict of interest.

## References

1. Dikin, D.A.; Stankovich, S.; Zimney, E.J.; Piner, R.D.; Dommett, G.H.; Evmenenko, G.; Nguyen, T.S.; Ruoff, R.S. Preparation and characterization of graphene oxide paper. *Nature* **2007**, *448*, 457-460, <https://doi.org/10.1038/nature06016>.
2. Stoller, M.D.; Park, S.; Zhu, Y.; An, J.; Ruoff, R.S. Graphene-based ultracapacitors. *Nano Lett.* **2008**, *8*, 3498-3502, <https://doi.org/10.1021/nl802558y>.
3. Yan, X.; Cui, X.; Li, B.; Li, L.S. Large solution-processable graphene quantum dots as light absorbers for photovoltaics. *Nano Lett.* **2010**, *10*, 1869-1873, <https://doi.org/10.1021/nl101060h>.
4. Razaq, A.; Bibi, F.; Zheng, X.; Papadakis, R.; Jafri, S.H.M.; Li, H. Review on graphene-, graphene oxide-, reduced graphene oxide-based flexible composites: From fabrication to applications. *Materials* **2022**, *15*, 1012, <https://doi.org/10.3390/ma15031012>.
5. Shen, J.; Zhu, Y.; Yang, X.; Zong, J.; Zhang, J.; Li, C. One-pot hydrothermal synthesis of graphene quantum dots surface-passivated by polyethylene glycol and their photoelectric conversion under near-infrared light. *New J. Chem.* **2012**, *36*, 97-101, <https://doi.org/10.1039/C1NJ20658C>.
6. Liu, Q.; Guo, B.; Rao, Z.; Zhang, B.; Gong, J.R. Strong two-photon-induced fluorescence from photostable, biocompatible nitrogen-doped graphene quantum dots for cellular and deep-tissue imaging. *Nano Lett.* **2013**, *13*, 2436-2441, <https://doi.org/10.1021/nl400368v>.
7. Yang, Y.; Zou, T.; Wang, Z.; Xing, X.; Peng, S.; Zhao, R.; Zhang, X.; Wang, Y. The Fluorescent Quenching Mechanism of N and S Co-Doped Graphene Quantum Dots with Fe<sup>3+</sup> and Hg<sup>2+</sup> Ions and Their Applications as a Novel Fluorescent Sensor. *Nanomaterials* **2019**, *9*, 738, <https://doi.org/10.3390/nano9050738>.
8. Du, Y.; Guo, S. Chemically doped fluorescent carbon and graphene quantum dots for bioimaging, sensor, catalytic and photoelectronic applications. *Nanoscale* **2016**, *8*, 2532-2543, <https://doi.org/10.1039/C5NR07579C>.
9. Lin, J.; Chen, X.; Huang, P. Graphene-based nanomaterials for bioimaging. *Adv. Drug Deliv. Rev.* **2016**, *105*, 242-254, <http://dx.doi.org/10.1016/j.addr.2016.05.013>.
10. Mousavi, S.M.; Hashemi, S.A.; Kalashgrani, M.Y.; Omidifar, N.; Bahrani, S.; Rao, N.V.; Babapoor, A.; Gholami, A.; Chiang, W.H. Bioactive Graphene Quantum Dots Based Polymer Composite for Biomedical Applications. *Polymers* **2022**, *14*, 617, <https://doi.org/10.3390/polym14030617>.
11. Akin, M.; Bekmezci, M.; Bayat, R.; Coguplugil, Z.K.; Sen, F.; Karimi, F.; Maleh, H.K. Mobile device integrated graphene oxide quantum dots based electrochemical biosensor design for detection of miR-141 as a pancreatic cancer biomarker. *Electrochimica Acta* **2022**, *435*, 141390, <https://doi.org/10.1016/j.electacta.2022.141390>.
12. Biswas, M.C.; Islam, M.T.; Nandy, P.K.; Hossain, M.M. Graphene Quantum Dots (GQDs) for bioimaging and drug delivery applications: a review. *ACS Mater. Lett.* **2021**, *3*, 889-911, <https://doi.org/10.1021/acsmaterialslett.0c00550>.

13. Regulska, E.; Breczko, J.; Basa, A.; Szydłowska, B.; Kakareko, K.; Rosołowska, A.R.; Hryszko, T. Graphene-quantum-dots-decorated NiAl<sub>2</sub>O<sub>4</sub> nanostructure as supercapacitor and electrocatalyst in biosensing. *Mater. Today Commun.* **2022**, *33*, 104166, <https://doi.org/10.1016/j.mtcomm.2022.104166>.
14. Hsiao, Y.C.; Hung, J.L.; Kubendhiran, S.; Yougbaré, S.; Lin, L.Y.; Wu, Y.F. Novel synthesis of N-doped graphene quantum dot as conductive agent for carbon based supercapacitors. *J. Energy Storage* **2022**, *56*, 105902, <https://doi.org/10.1016/j.est.2022.105902>.
15. Prabhakar, A.K.; Ajith, M.P.; Ananthanarayanan, A.; Routh, P.; Mohan, B.C.; Thamizchelvan, A.M. Ball-milled graphene quantum dots for enhanced anti-cancer drug delivery. *OpenNano* **2022**, *8*, 100072, <https://doi.org/10.1016/j.onano.2022.100072>.
16. Cala, B.F.; Soriano, M.L.; Sciortino, A.; Cannas, M.; Messina, F.; Cardenas, S. One-pot synthesis of graphene quantum dots and simultaneous nanostructured self-assembly via a novel microwave-assisted method: impact on triazine removal and efficiency monitoring. *RSC Adv.* **2018**, *8*, 29939-29946, <https://doi.org/10.1039/C8RA04286A>.
17. Zhao, L.; Wang, Y.; Li, Y. Antioxidant activity of graphene quantum dots prepared in different electrolyte environments. *Nanomaterials* **2019**, *9*, 1708. <https://doi.org/10.3390/nano9121708>.
18. Cao, H.; Qi, W.; Gao, X.; Wu, Q.; Tian, L.; Wu, W. Graphene Quantum Dots prepared by Electron Beam Irradiation for Safe Fluorescence Imaging of Tumor. *Nanotheranostics* **2022**, *6*, 205-214, <https://doi.org/10.7150/ntno.67070>.
19. Shehab, M.; Ebrahim, S.; Soliman, M. Graphene quantum dots prepared from glucose as optical sensor for glucose. *J. Lumin.* **2017**, *184*, 110-116, <https://doi.org/10.1016/j.jlumin.2016.12.006>.
20. Sun, Y.; Wang, S.; Li, C.; Luo, P.; Tao, L.; Wei, Y.; Shi, G. Large scale preparation of graphene quantum dots from graphite with tunable fluorescence properties. *Phys. Chem. Chem. Phys.* **2013**, *15*, 9907-9913, <https://doi.org/10.1039/C3CP50691F>.
21. Zhang, Y.; Li, K.; Ren, S.; Dang, Y.; Liu, G.; Zhang, R.; Zhang, K.; Long, X.; Jia, K. Coal-derived graphene quantum dots produced by ultrasonic physical tailoring and their capacity for Cu (II) detection. *ACS Sustainable Chem. Eng.* **2019**, *7*, 9793-9799, <https://doi.org/10.1021/acssuschemeng.8b06792>.
22. Xu, Q.; Gong, Y.; Zhang, Z.; Miao, Y.; Li, D.; Yan, G. Preparation of graphene oxide quantum dots from waste toner, and their application to a fluorometric DNA hybridization assay. *Microchim. Acta* **2019**, *186*, 1-7, <https://doi.org/10.1007/s00604-019-3539-x>.
23. Stankovich, S.; Dikin, D.A.; Piner, R.D.; Kohlhaas, K.A.; Kleinhammes, A.; Jia, Y.; Wu, Y.; Nguyen, S.T.; Ruoff, R.S. Synthesis of graphene-based nanosheets via chemical reduction of exfoliated graphite oxide. *Carbon* **2007**, *45*, 1558-1565, <https://doi.org/10.1016/j.carbon.2007.02.034>.
24. Roy, P.; Periasamy, A.P.; Chuang, C.; Liou, Y.R.; Chen, Y.F.; Joly, J.; Liang, C.T.; Chang, H.T. Plant leaf-derived graphene quantum dots and applications for white LEDs. *New J. Chem.* **2014**, *38*, 4946-4951, <https://doi.org/10.1039/C4NJ01185F>.
25. Revathi, V.; Karthik, K. Microwave assisted CdO-ZnO-MgO nanocomposite and its photocatalytic and antibacterial studies. *J. Mater. Sci. Mater. Electron.* **2018**, *29*, 18519-18530, <https://doi.org/10.1007/s10854-018-9968-1>.
26. Qu, J.; Luo, C.; Hou, J. Synthesis of ZnO nanoparticles from Zn-hyperaccumulator (*Sedum alfredii* Hance) plants. *Micro Nano Lett.* **2011**, *6*, 174-176, <https://doi.org/10.1049/mnl.2011.0004>.
27. Phophayu, S.; Pimpang, P.; Wongrerkdee, S.; Sujinnapram, S.; Wongrerkdee, S. Modified graphene quantum dots-zinc oxide nanocomposites for photocatalytic degradation of organic dyes and commercial herbicide. *J. Reinf. Plast. Compos.* **2020**, *39*, 81-94. <https://doi.org/10.1177/0731684419891245>.
28. Liu, J.; Shao, J.; Wang, Y.; Li, J.; Liu, H.; Wang, A.; Hui, A.; Chen, S. Antimicrobial activity of zinc oxide-graphene quantum dot nanocomposites: enhanced adsorption on bacterial cells by cationic capping polymers. *ACS Sustain. Chem. Eng.* **2019**, *7*, 16264-16273, <https://doi.org/10.1021/acssuschemeng.9b03292>.
29. Kharkwal, A.; Purohit, G.; Rawat, D.S. Zinc Oxide Sensitized Graphene Quantum Dots "ZnO-GQDs": A Hybrid Concept to Study Charge Transfer and its Catalytic Applicability to Synthesize Tetrasubstituted Propargylamines. *Asian J. Org. Chem.* **2020**, *9*, 2162-2169, <https://doi.org/10.1002/ajoc.202000460>.
30. Mydeen, S.S.; Kumar, R.R.; Sivakumar, R.; Sambathkumar, S.; Kottaisamy, M.; Vasantha, V.S. Graphene quantum dots/ZnO nanocomposite: Synthesis, characterization, mechanistic investigations of photocatalytic and antibacterial activities. *Chem. Phys. Lett.* **2020**, *761*, 138009, <https://doi.org/10.1016/j.cplett.2020.138009>.
31. Zhou, Z.; Pourhashem, S.; Wang, Z.; Duan, J.; Zhang, R.; Hou, B. Distinctive roles of graphene oxide, ZnO quantum dots, and their nanohybrids in anti-corrosion and anti-fouling performance of waterborne epoxy coatings. *Chem. Eng. J.* **2022**, *439*, 135765, <https://doi.org/10.1016/j.cej.2022.135765>.

32. Chong, Y.; Ge, C.; Fang, G.; Tian, X.; Ma, X.; Wen, T.; Wamer, W.G.; Chai, Z.; Yin, J.J. Crossover between anti-and pro-oxidant activities of graphene quantum dots in the absence or presence of light. *ACS Nano* **2016**, *10*, 8690-8699, <https://doi.org/10.1021/acsnano.6b04061>.
33. Wang, M.; Chen, J.; Liu, C.; Qiu, J.; Wang, X.; Chen, P.; Xu, C. A graphene quantum dots-hypochlorite hybrid system for the quantitative fluorescent determination of total antioxidant capacity. *Small* **2017**, *13*, 1700709, <https://doi.org/10.1002/smll.201700709>.
34. Jayanthi, P.; Lalitha, P. Reducing power of the solvent extracts of *Eichhornia crassipes* (Mart.) Solms. *Int. J. Pharm. Pharm. Sci.* **2011**, *3*, 126-128, <https://innovareacademics.in/journal/ijpps/Vol3Suppl3/2155.pdf>.
35. Gorrini, C.; Harris, I.S.; Mak, T.W. Modulation of oxidative stress as an anticancer strategy. *Nat. Rev. Drug Discov.* **2013**, *12*, 931-947, <https://doi.org/10.1038/nrd4002>.
36. Kumar, N.; Singh, A.; Sharma, D.K.; Kishore, K. *In-Vitro* anti inflammatory and antioxidant activity of *Onosma hispidum* (Ratanjot) Roots. *Int. J. Pharm. Biol. Sci.* **2017**, *3*, 30-35, [https://www.ijpbs.com/ijpbsadmin/upload/ijpbs\\_59e0984bc1584.pdf](https://www.ijpbs.com/ijpbsadmin/upload/ijpbs_59e0984bc1584.pdf).
37. Ayoka, T.O.; Ezema, B.O.; Eze, C.N.; Nnadi, C.O. Antioxidants for the Prevention and Treatment of Non-communicable Diseases. *J. Explor. Res. Pharmacol.* **2022**, *7*, 178-188, <https://doi.org/10.14218/JERP.2022.00028>.
38. Tamma, P.D.; Cosgrove, S.E.; Maragakis, L.L. Combination Therapy for Treatment of Infections with Gram-Negative Bacteria. *Clin. Microbiol. Rev.* **2012**, *25*, 450-470, <https://doi.org/10.1128/CMR.05041-11>.
39. Sun, M.; Qu, A.; Hao, C.; Wu, X.; Xu, L.; Xu, C.; Kuang, H. Chiral Upconversion Heterodimers for Quantitative Analysis and Bioimaging of Antibiotic-Resistant Bacteria In Vivo. *Adv. Mater.* **2018**, *30*, 1804241, <https://doi.org/10.1002/adma.201804241>.
40. Rai, M.; Yadav, A.; Gade, A. Silver nanoparticles as a new generation of antimicrobials. *Biotechnol. Adv.* **2009**, *27*, 76-83, <https://doi.org/10.1016/j.biotechadv.2008.09.002>.
41. Kahraman, O.; Binzet, R.; Turunc, E.; Dogen, A.; Arslan, H. Synthesis, characterization, antimicrobial and electrochemical activities of zinc oxide nanoparticles obtained from *Sarcopoterium spinosum* (L.) Spach leaf extract. *Mater. Res. Express* **2018**, *5*, 115017, <https://doi.org/10.1088/2053-1591/aad953>.
42. Loo, Y.Y.; Rukayadi, Y.; Nor-Khaizura, M.A.R.; Kuan, C.H.; Chieng, B.W.; Nishibuchi, M.; Radu, S. *In vitro* antimicrobial activity of green synthesized silver nanoparticles against selected gram-negative foodborne pathogens. *Front. Microbiol.* **2018**, *9*, 1555, <https://doi.org/10.3389/fmicb.2018.01555>.
43. El-Gendy, A.O.; Nawaf, K.T.; Ahmed, E.; Samir, A.; Hamblin, M.R.; Hassan, M.; Mohamed, T. Preparation of zinc oxide nanoparticles using laser-ablation technique: Retinal epithelial cell (ARPE-19) biocompatibility and antimicrobial activity when activated with femtosecond laser. *J. Photochem. Photobiol. B* **2022**, *234*, 112540, <https://doi.org/10.1016/j.jphotobiol.2022.112540>.
44. Staron, A.; Dlugosz, O. Antimicrobial properties of nanoparticles in the context of advantages and potential risks of their use. *J. Environ. Sci. Health A* **2021**, *56*, 680-693, <https://doi.org/10.1080/10934529.2021.1917936>.
45. Elyasiyan, U.; Nudel, A.; Skalka, N.; Rozenberg, K.; Drori, E.; Oppenheimer, R.; Kerem, Z.; Rosenzweig, T. Anti-diabetic activity of aerial parts of *Sarcopoterium spinosum*. *BMC Complement. Altern. Med.* **2017**, *17*, 1-12, <https://doi.org/10.1186/s12906-017-1860-7>.
46. Henkin, Z.; Seligman, N.G. Survival of *Sarcopoterium spinosum* seedlings growing on terra rossa soil. *Isr. J. Plant Sci.* **2007**, *55*, 45-51, <https://www.tandfonline.com/doi/abs/10.1560/IJPS.55.1.45?journalCode=tips20>.
47. Yaniv, Z.; Dafni, A.; Friedman, J.; Palevitch, D. Plants used for the treatment of diabetes in Israel. *J. Ethnopharmacol.* **1987**, *19*, 145-151, [https://doi.org/10.1016/0378-8741\(87\)90038-9](https://doi.org/10.1016/0378-8741(87)90038-9).
48. Ali-Shtayeh, M.S.; Yaniv, Z.; Mahajna, J. Ethnobotanical Survey in the Palestinian area: a classification of the healing potential of medicinal plants. *J. Ethnopharmacol.* **2000**, *73*, 221-232, [https://doi.org/10.1016/S0378-8741\(00\)00316-0](https://doi.org/10.1016/S0378-8741(00)00316-0).
49. Ruch, R.J.; Cheng, S.J.; Klaunig, J.E. Prevention of cytotoxicity and inhibition of intercellular communication by antioxidant catechins isolated from Chinese green tea. *Carcinogenesis* **1989**, *10*, 1003-1008, <https://doi.org/10.1093/carcin/10.6.1003>.
50. Hue, S.M.; Boyce, A.N.; Somasundram, C. Antioxidant activity, phenolic and flavonoid contents in the leaves of different varieties of sweet potato (*Ipomoea batatas*). *Aust. J. Crop Sci.* **2012**, *6*, 375-380, <https://search.informit.org/doi/abs/10.3316/INFORMIT.351090686652014>.
51. Sahgal, G.; Ramanathan, S.; Sasidharan, S.; Mordi, M.N.; Ismail, S.; Mansor, S.M. *In vitro* antioxidant and xanthine oxidase inhibitory activities of methanolic *Swietenia mahagoni* seed extracts. *Molecules* **2009**, *14*, 4476-4485, <https://doi.org/10.3390/molecules14114476>.

52. Albayrak, F.; Çiçek, M.; Alkaya, D.; Kulu, I. Design, synthesis and biological evaluation of 8-aminoquinoline-1, 2, 3-triazole hybrid derivatives as potential antimicrobial agents. *Med. Chem. Res.* **2022**, *31*, 652-665, <https://doi.org/10.1007/s00044-022-02866-2>.
53. Kumar, R.; Anandan, S.; Hembram, K.; Rao, T.N. Efficient ZnO-based visible-light-driven photocatalyst for antibacterial applications. *ACS Appl. Mater. Interfaces* **2014**, *6*, 13138-13148, <https://doi.org/10.1021/am502915v>.
54. Tashkhourian, J.; Nami-Ana, S.F.; Shamsipur, M. Designing a modified electrode based on graphene quantum dot-chitosan application to electrochemical detection of epinephrine. *J. Mol. Liq.* **2018**, *266*, 548-556, <https://doi.org/10.1016/j.molliq.2018.06.093>.
55. Sarkar, S.; Gandla, D.; Venkatesh, Y.; Bangal, P.R.; Ghosh, S.; Yang, Y.; Misra, S. Graphene quantum dots from graphite by liquid exfoliation showing excitation-independent emission, fluorescence upconversion and delayed fluorescence. *Phys. Chem. Chem. Phys.* **2016**, *18*, 21278-21287, <https://doi.org/10.1039/c6cp01528j>.
56. Tayyebi, A.; Outokesh, M.; Tayebi, M.; Shafikhani, A.; Şengör, S.S. ZnO quantum dots-graphene composites: Formation mechanism and enhanced photocatalytic activity for degradation of methyl orange dye. *J. Alloys Compd.* **2016**, *663*, 738-749, <https://doi.org/10.1016/j.jallcom.2015.12.169>.
57. Xu, T.; Zhang, L.; Cheng, H.; Zhu, Y. Significantly enhanced photocatalytic performance of ZnO via graphene hybridization and the mechanism study. *Appl. Catal. B* **2011**, *101*, 382-387, <https://doi.org/10.1016/j.apcatb.2010.10.007>.
58. Vanzetti, L.; Pasquardini, L.; Potrich, C.; Vaghi, V.; Battista, E.; Causa, F.; Pederzoli, C. XPS analysis of genomic DNA adsorbed on PEI- modified surfaces. *Surf. Interface Anal.* **2016**, *48*, 611-615, <https://doi.org/10.1002/sia.5932>.
59. Claros, M.; Setka, M.; Jimenez, Y.P.; Vallejos, S. AACVD synthesis and characterization of iron and copper oxides modified ZnO structured films. *Nanomaterials* **2020**, *10*, 471, <https://doi.org/10.3390/nano10030471>.
60. Das, T. K.; Wati, M.R.; Shad, K.F. Oxidative stress gated by Fenton and Haber Weiss reactions and its association with Alzheimer's disease. *Arch. Neurosci.* **2015**, *2*, e20078, <https://doi.org/10.5812/archneurosci.20078>.
61. Firuzi, O.; Lacanna, A.; Petrucci, R.; Marrosu, G.; Saso, L. Evaluation of the antioxidant activity of flavonoids by "ferric reducing antioxidant power" assay and cyclic voltammetry. *Biochim. Biophys. Acta - Gen. Subj.* **2005**, *1721*, 174-184, <https://doi.org/10.1016/j.bbagen.2004.11.001>.
62. Candan, F. Effect of *Rhus coriaria* L. (Anacardiaceae) on superoxide radical scavenging and xanthine oxidase activity. *J. Enzyme Inhib. Med. Chem.* **2003**, *18*, 59-62, <https://doi.org/10.1080/1475636031000069273>.
63. Mittal, A.; Phillips, A.R.; Loveday, B.; Windsor, J.A. The potential role for xanthine oxidase inhibition in major intra-abdominal surgery. *World J. Surg.* **2008**, *32*, 288-295, <https://doi.org/10.1007/s00268-007-9336-4>.
64. Kelley, E.E.; Khoo, N.K.; Hundley, N.J.; Malik, U.Z.; Freeman, B.A.; Tarpey, M.M. Hydrogen peroxide is the major oxidant product of xanthine oxidase. *Free Radic. Biol. Med.* **2010**, *48*, 493-498, <https://doi.org/10.1016/j.freeradbiomed.2009.11.012>.
65. Flemmig, J.; Kuchta, K.; Arnhold, J.; Rauwald, H.W. *Olea europaea* leaf (Ph. Eur.) extract as well as several of its isolated phenolics inhibit the gout-related enzyme xanthine oxidase. *Phytomedicine* **2011**, *18*, 561-566, <https://doi.org/10.1016/j.phymed.2010.10.021>.
66. Choi, H.K.; Mount, D.B.; Reginato, A.M. Pathogenesis of gout. *Ann. Intern. Med.* **2005**, *143*, 499-516, <https://doi.org/10.7326/0003-4819-143-7-200510040-00009>.
67. Tian, J.; Shen, S.; Zhou, C.; Dang, X.; Jiao, Y.; Li, L.; Ding, S.; Li, H. Investigation of the antimicrobial activity and biocompatibility of magnesium alloy coated with HA and antimicrobial peptide. *J. Mater. Sci. Mater. Med.* **2015**, *26*, 1-12, <https://doi.org/10.1007/s10856-015-5389-3>.
68. Haider, A.; Ijaz, M.; Imran, M.; Naz, M.; Majeed, H.; Khan, J.A.; Ali, M.M.; Ikram, M. Enhanced bactericidal action and dye degradation of spicy roots' extract-incorporated fine-tuned metal oxide nanoparticles. *Appl. Nanosci.* **2020**, *10*, 1095-1104, <https://doi.org/10.1007/s13204-019-01188-x>.
69. Prasanna, V.L.; Vijayaraghavan, R. Insight into the mechanism of antibacterial activity of ZnO: surface defects mediated reactive oxygen species even in the dark. *Langmuir* **2015**, *31*, 9155-9162, <https://doi.org/10.1021/acs.langmuir.5b02266>.
70. Kadian, S.; Manik, G.; Das, N.; Nehra, P.; Chauhan, R.P.; Roy, P. Synthesis, characterization and investigation of synergistic antibacterial activity and cell viability of silver-sulfur doped graphene quantum dot (Ag@S-GQDs) nanocomposites. *J. Mater. Chem. B* **2020**, *8*, 3028-3037, <https://doi.org/10.1039/C9TB02823D>.



71. Rajaura, R.S.; Sharma, V.; Ronin, R.S.; Gupta, D.K.; Srivastava, S.; Agrawal, K.; Vijay, Y.K. Synthesis, characterization and enhanced antimicrobial activity of reduced graphene oxide–zinc oxide nanocomposite. *Mater. Res. Express* **2017**, *4*, 025401, <https://doi.org/10.1088/2053-1591/aa5bff>.
72. Usman, O.; Ikram, M.; Abid, N.; Saeed, M.; Bashir, A.; Nabgan, W.; Mushadid, N.; Ikram, M. Enhanced Bactericidal Action of rGO-ZnO Hybrids Prepared by the One-Pot Co-precipitation Approach. *ACS Omega*. **2022**, *30*, 26715-26722, <https://doi.org/10.1021/acsomega.2c03049>.
73. Gao, D.; Zhao, P.; Lyu, B.; Li, Y.; Hou, Y.; Ma, J. Carbon quantum dots decorated on ZnO nanoparticles: An efficient visible-light responsive antibacterial agents. *Appl. Organomet. Chem.* **2020**, *34*, e5665, <https://doi.org/10.1002/aoc.5665>.
74. Safardoust-Hojaghan, H.; Salavati-Niasari, M.; Amiri, O.; Rashki, S.; Ashrafi, M. Green synthesis, characterization and antimicrobial activity of carbon quantum dots-decorated ZnO nanoparticles. *Ceram. Int.* **2021**, *47*, 5187-5197, <https://doi.org/10.1016/j.ceramint.2020.10.097>.